Geoderma 320 (2018) 161–171

Contents lists available at ScienceDirect

Geoderma

journal homepage: www.elsevier.com/locate/geoderma

Effects of three morphometric features of roots on soil water flow behavior in three sites in China

Xiao Jin Jiang[a,*], Wenjie Liu[a,*], Chunfeng Chen[a,b], Jiaqing Liu[a,b], Zi-Qiang Yuan[c], Baocheng Jin[d], Xiayang Yu[e]

[a] Key Laboratory of Tropical Forest Ecology, Xishuangbanna Tropical Botanical Garden, Chinese Academy of Sciences, Menglun, Yunnan 666303, PR China
[b] University of Chinese Academy of Sciences, Beijing 100049, PR China
[c] State Key Laboratory of Frozen Soil Engineering, Northwest Institute of Eco-environment and Resources, Chinese Academy of Science, Lanzhou, Gansu 730000, PR China
[d] College of Animal Science, Guizhou University, Guiyang, Guizhou 550025, PR China
[e] State Key Laboratory of Hydrology-Water Resources and Hydraulic Engineering, Hohai University, Nanjing, Jiangsu 210098, PR China

ARTICLE INFO

Keywords:
Preferential flow
Matrix flow
Rhizopore
Dye tracer
Capillary force

ABSTRACT

Soil physical properties, infiltrability, and water flow behavior are closely associated with root morphology. In this study, dye tracer experiments were conducted in the field to assess the effects of roots with various morphometric features on soil water flow behavior and soil infiltrability. Preferential flow is the dominant type of water flow in the three study sites (Minqin, Dongtai, and Mengla). The presence of roots caused noncapillary porosity and saturated hydraulic conductivity to increase by 26% and 252% in the Minqin, 92% and 93% in the Dongtai, and 234% and 96% in the Mengla, respectively, relative to that in in soils without roots. The various morphometric features of roots affect water flow behavior in soil. The fibrous roots of maize induced water to flow and distribute evenly throughout the plough layer of the study site in Minqin. Furrows and ridges in this site exhibited different soil physical and hydrological properties. Furrows could store higher amounts of water than ridges, thereby increasing the likelihood of water absorption by plants. In Dongtai, ponding and surface runoff occurred when water infiltration was inhibited by the mud layer, which exhibited a high soil bulk density value of 1.43 g cm^{-3} and a low saturated hydraulic conductivity value of 1.67×10^{-5} cm s^{-1}. These phenomena were not observed in plots the smooth roots of *Spartina alterniflora* penetrated the mud layer. In this site, preferential flow and lateral flow, which is triggered by the sandy loam layer, are important for water discharge from the beach to the ocean. In Mengla, water flowed evenly on hard soil, which exhibited a high bulk density value of 1.43 g cm^{-3}. The fine roots of rubber could guide water infiltration into deep soil layers (73.54 cm), thereby redistributing water to the root zones of rubber trees. Therefore, our findings indicated that water infiltration behavior, which is crucial for water distribution, is affected by the various morphometric features of roots.

1. Introduction

Water infiltration through soil is associated with surface runoff, soil erosion, plant water storage, and groundwater recharge (Lipiec et al., 2006). In addition to water infiltration amount, water flow behavior is increasingly recognized as a major factor of water distribution in soils (Jiang et al., 2017c).

Types of water infiltration through soil generally include matrix and preferential flows. Matrix flow is defined as the slow movement of water and solutes through bulk soil (Allaire et al., 2009). Preferential flow is defined as the physical movement of water and solutes along certain pathways while bypassing a fraction of the pore matrix (Hendrickx and Flury, 2001). In this case, water and solutes move to far greater depths than the depths predicted through Richards' equation, which is based on area-averaged moisture contents and pressure heads (Beven and Germann, 1982). Preferential flow occurs in most soils and is often attributed to macropore flow through cracks, fissures, or voids and between peds or through biopores, such as earthworm burrows, roots channels, and crab burrows (Flury and Flühler, 1995; Xin et al., 2016). Preferential flow in soils does not only result from macropore flow but also from on-homogeneous infiltration, lateral flow, and wetting front instabilities (Allaire et al., 2009; Bundt et al., 2001). Lateral flow refers to the infiltration of laterally moving water (Oostindie et al., 2013; Ritsema and Dekker, 1995; Wine et al., 2012). Dye tracers may be used to visualize preferential flow paths in soils (Flury and Flühler, 1994; Ghodrati and Jury, 1990). Dye patterns could

* Corresponding author.
E-mail addresses: jiangxiaojinlinda@163.com (X.J. Jiang), lwj@xtbg.org.cn (W. Liu).

https://doi.org/10.1016/j.geoderma.2018.01.035
Received 10 October 2017; Received in revised form 17 January 2018; Accepted 28 January 2018
Available online 06 February 2018
0016-7061/

be classified by processing the original dye-stained soil profiles through image analysis programs. Thus, different types of water flow behavior (e.g., preferential flow and lateral flow) and their quantitative information (e.g., dye-stained width, depth, and area) can be directly interpreted from the classified dye patterns (Cey and Rudolph, 2009; Ghodrati and Jury, 1990).

Water infiltration in soil is affected by several external factors, such as tillage and management practice (Jiang et al., 2017a; McGarry et al., 2000); vegetation cover and soil texture (Castellano and Valone, 2007); and compaction through trampling by livestock, traffic, and machines (Fleischner, 1994; Wang et al., 2015). Moreover, internal factors, such as soil structure, water repellency, soil bulk density, thermal conductivity, evapotranspiration rates, and soil microorganisms could affect soil water infiltration (Bond, 1964; Bond and Harris, 1964; Czarnes et al., 2000; DeBano et al., 1977). Other factors that affect soil water infiltration include the formation of ash particles resulted from vegetation fires (Mallik et al., 1984); incorporation of objects (e.g., residual plastic film, straw, and stones) into soil (Jiang et al., 2017b; Kodešová et al., 2012; Laine-Kaulio et al., 2015); features of roots (Gibbs and Reid, 1988); channels of roots (Beven and Germann, 1982; Flury and Flühler, 1995); and soil fauna (Tebrügge and Düring, 1999).

The influenced of roots and their morphometric features on preferential flow should be considered. Old roots channels that have openings at the soil surface (Wang and Strong, 1996) and decaying roots that appear at deep penetration depths in the vertical direction (Mitchell, 1995) are considered as soil macropores. Roots channels are a type of macropore with specific properties, organization, kinetics, and control factors. Root architecture and traits, such as diameter, length, orientation, topology, sinuosity, and decay rate, influence the creation of roots channels and thus affect preferential flow. In particular, root diameter can be smaller than rhizopore diameter, thus presenting a cylindrical space for potential water flow (Ghestem et al., 2011). In addition, fibrous or smooth roots could induce different kinds of water infiltration behavior. However, the effects of roots with different morphometric features on water infiltration characteristics through soil have never been reported in the literature. Thus, the effects of roots on water infiltration behavior should be monitored and quantified. In this study, we selected three kinds of roots with various morphometric features from three sites. In addition to acquiring soil physical property (e.g., bulk density and porosity) measurements, we conducted dye tracer experiments to simultaneously measure water infiltrability and trace water movement in soil. Moreover, we aimed to reveal the ecological significance of water infiltration behavior in the three study sites.

2. Materials and methods

2.1. Morphometric features of roots

The features of roots in three sites (Minqin, Dongtai, and Mengla) are shown in Fig. 1. The majority of the biomass of the fibrous roots of maize (*Zea mays* L.) was confined to the upper 20 cm soil layer. The smooth roots of *Spartina alterniflora* easily penetrated soil (Fig. 1 middle). The fine roots of rubber tree (*Hevea brasiliensis*) were primarily distributed in the upper 30 cm soil layer (Fig. 1 right). The root biomass per plot at each site is presented in Fig. 2.

2.2. Experimental site and design

To reveal the ecological significance of water infiltration behavior in various soils, different sites with special roots features were selected, namely Minqin having the fibrous roots of maize, Dongtai having the smooth roots of *Spartina alterniflora*, and Mengla having the fine roots of rubber tree (Fig. 3). The geographic locations and soil particle size distributions of the sites are provided in Table 1.

The Minqin Oasis is located in the northwest Gansu Province of China. The site has an arid continental climate with an average annual temperature of 7.8 °C. The mean precipitation and the average evaporation in the area is 110.5 mm year^{-1} and 2646.4 mm year^{-1}, respectively. Soils at the site developed from alluvial sediments with > 100 cm in depth. Its soil is classified as Anthropic Camborthids (IUSS Working Group WRB, 2014) (Fig. 3. I). The study site is under ridge-furrow cropping and is fully mulched with plastic film. It is cultivated with various crops, such as maize and sunflower. A detailed description of the experimental site is given in Jiang et al. (2017b). Loose top soil layers of 2 cm and 12 cm were carefully removed from the furrows and ridges, respectively, to prepare quadrants with horizontal surfaces. Center quadrants in the furrows matched sites of roots growth. Center quadrants in the wide ridge matched axle wires. Three quadrants with roots in the furrows were randomly selected as the roots plot, whereas three other quadrants without roots in the ridges were randomly selected as the no roots plot (Fig. 4. B). All quadrants were prepared from May 5 to 15 (2014), which corresponded to the jointing stage of spring maize (the roots was not large enough to stretch in ridges).

Dongtai is located in the central Jiangsu Province of China. The site has a monsoon climate ranging from warm-temperate to northern subtropical. The mean annual precipitation and temperature of the site is 1022.9 mm and 14.36 °C, respectively. The muddy flats in the site are even, with widths of 2–6 km. The widest width is 13 km. The width of the upper mudflat, which is suitable for *S. alterniflora* growth, is between 1 and 4 km. The soil under study is classified as Saline-alkaline (IUSS Working Group WRB, 2014) with alternating sandy loam and mud layers (Fig. 3. II). *S. alterniflora* seeds are carried by tidal waves to the higher flats of northwestern Tiaozini, where they germinate. Field observations showed that the *S. alterniflora* clump area was 5–30 m^2 with a mean density of 50–70 culms m^{-2}. Mean culm height was 1.0 m (maximum 2.0 m), and mean culm diameter was 0.45 cm. Single or several seedlings and small clumps sparsely grow around the external margins of the clump area, and three quadrants were randomly selected as the roots plot. Meanwhile, the other three quadrants (100 m to the sea), which were distance from the clump area, were randomly selected as the no roots plot (Fig. 5. B). All quadrants were prepared from April 10 to 20, 2015.

Mengla County is located in the southern Yunnan Province of China. The local climate is dominated by tropical southern monsoons from the Indian Ocean between May and October and subtropical jet streams between November and April. This area experiences three seasons: rainy, foggy cool, and hot dry. Climate records over the past 40 years showed that the area has a mean annual air temperature of 21.7 °C and mean annual rainfall of 1487 mm. Most of the precipitation (87%) occurs between May and October. The soil depth under vegetation is approximately 2 m. The soil in the study area is well drained and has a clay loam texture. The soil is classified as Ferralic Cambisol (IUSS Working Group WRB, 2014) that developed from alluvial deposits derived from sandstones. It exhibits an ochric A horizon and a cambic B horizon with ferralic properties (Vogel et al., 1995) (Fig. 3. III). A typical field with a land area of 60 m × 18 m and planted with 50-year-old rubber trees (clone PB86) was selected for this study. Owing to long-term cultivation and management measures, the field has a terrain slope of nearly 0°. Rubber trees were arranged 2 m apart in double rows, which were 3 m apart, and each set of double rows was separated by a gap 18 m in width. Roots and biomass changed along with the distance from the axle wire between two rows to rubber planted rows. Almost no roots were observed in the axle wire between two rows (18 m wide gap); thus, three quadrants within the axle wire (9 m to rubber tree) were randomly selected as the no roots plot. Meanwhile, the other three quadrants, which were 4 m to the nearest rubber tree, were selected as the roots plot (Fig. 6. B). All quadrants were prepared from October 1 to 10, 2016.

Fig. 1. Different morphometric features of roots. Fibrous roots for maize in Minqin (left), smooth roots for *S. alterniflora* in Dongtai (middle), and fine roots for rubber in Mengla (right).

2.3. Dye tracer infiltration

Eighteen dye tracer experiments were conducted on the above quadrants (50 cm × 50 cm, 3 m away from each other in one site) to measure water infiltration rate and visualize the water flow path. In each test quadrant, we placed a single hollow cylinder made of stainless steel (diameter, 0.2 m; height, 0.3 m). The bottom edges of the cylinder were inserted 0.05 m into the soil, and its side walls and edges were water tight. Tap water was dyed with Brilliant Blue FCF at a concentration of 4.0 g L^{-1} (Flury and Flühler, 1995). Each cylinder was initially filled with dye water equivalent to a water head of 5.0 cm. The time taken for the water level to decrease to 1.0 cm in the cylinder was recorded. Thereafter, a measured volume of water, equivalent to 1.0 cm in depth, was successively added to the cylinder until the infiltration time did not change for three consecutive measurements taken at 5-min intervals. Steady-state flow was assumed at this point, and the steady-state infiltration rate (I_s) was calculated on the basis of the last three measurements (Bodhinayake et al., 2004). Using the steady state infiltration rate (I_s, 10 °C), the field hydraulic conductivity of saturated soil (K_s cm s^{-1}) was calculated in accordance with the following equation (Reynolds and Elrick, 1990):

$$K_S = \frac{I_S}{\left[\left(\frac{H}{C_1 d + C_2 a}\right) + \left(\frac{1}{\alpha(C_1 d + C_2 a)}\right)\right] + 1}$$

where I_s is the quasi-steady state infiltration rate in cm s^{-1}, H is the average ponding depth in cm, a is the radius of the inner cylinder in cm, d is the insertion depth of the cylinder into the soil in cm, C_1 and C_2 are dimensionless quasiempirical constants, and α is the soil macroscopic capillary length. For this work a, d and α were 10 cm, 5 cm, and 0.12 cm^{-1}, respectively. The constants C_1 and C_2 were 0.316π and 0.184π, respectively, for $d \geq 3$ cm and $H \geq 5$ cm (Reynolds and Lewis, 2012). The value of H for each run was calculated from the final filling event as the average between the highest water level and the lowest

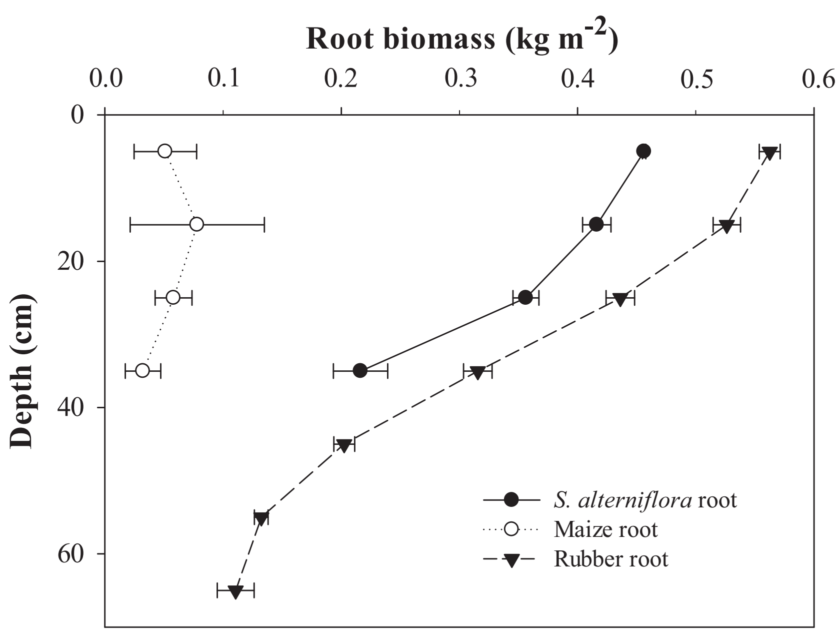

Fig. 2. Root biomass distribution in the soil profile for plots with roots. Data are expressed as means ± standard error (n = 3).

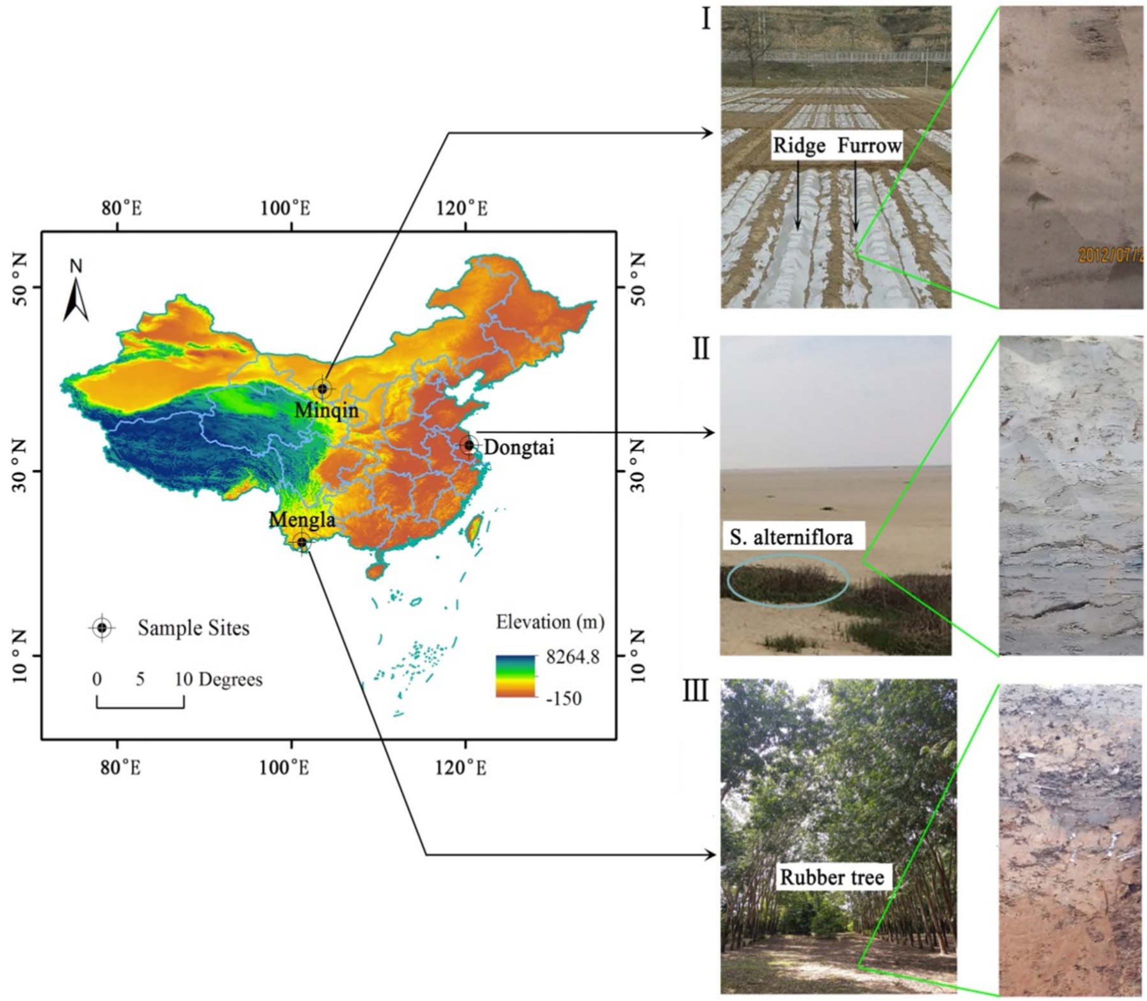

Fig. 3. Map showing the location of the three study sites of and soil profiles in China. I: Pattern of plastic film fully-mulched ridge-furrow cropping applied to planting crops in Minqin which exhibited a more homogeneous soil profile. II: The patch distribution patterns of *S. alterniflora* in the mudflat of Dongtai exhibited alternating sandy loam layers (thickness: 12 cm) and mud layers (thickness: 3 cm). III: Rubber tree was expanded as monoculture crop systems in Mengla, which exhibited an ochric A horizon and a cambic B horizon.

water level, which was fixed at 5 cm.

After infiltration was completed, the quadrants were immediately covered with large plastic sheets to prevent soil evaporation and dilution by rainfall (Jiang et al., 2015). Twenty-four hours after the end of infiltration, 70 cm (width) × 60 cm (depth) dye-stained vertical soil sections were carefully excavated from the center of the cylinder using a spatula (Weiler and Flühler, 2004). The calibrated frames of the vertical soil sections were placed in the soil profile to facilitate image correction. Eighteen soil sections were photographed using a digital camera (Canon EOS Rebel T3, Japan). The distance from the camera to the center of the vertical soil section was 50 cm. All areas of the pit were covered with a black umbrella to provide a soft light condition. Dye-stained calibration patches were prepared for the imaging of soil horizons as described by Weiler and Flühler (2004) to define the concentration categories for dye-stained soil regions during image analysis. Immediately after photographing, a spatula was used to acquire soil samples from dyed regions of the eighteen vertical soil sections using from each plot. The subsoil samples were pooled to form one composite

Table 1
Soil properties (mean ± SE, n = 3) and geographic location of the experimental sites.

Site	amsl (m)	Geographical coordinates	Soil layer (cm)	Particle size		
				Clay (%)	Silt (%)	Sand (%)
Minqin	1298–1936	101°49′–104°12′E; 38°03′–39°28′N	0—20	10.8	40.0	49.2
			20—40	12.8	38.9	48.3
Dongtai	1.4–5.1	120°07′–120°53′E; 32°33′–32°57′N	Sandy loam layer[a]	15.4	18.1	66.5
			Mud layer[b]	55.1	25.2	19.7
Mengla	480–2030	101°05′–101°50′E; 21°09′–22°23′N	0—20	29.0	30.3	40.7
			20—40	26.9	32.7	40.4
			40—60	23.6	34.6	41.8
			60—80	17.4	36.6	46.0

[a] Soil depths was 0—12 cm and 15—27 cm.
[b] Soil depths was 12—15 cm 27—30 cm.

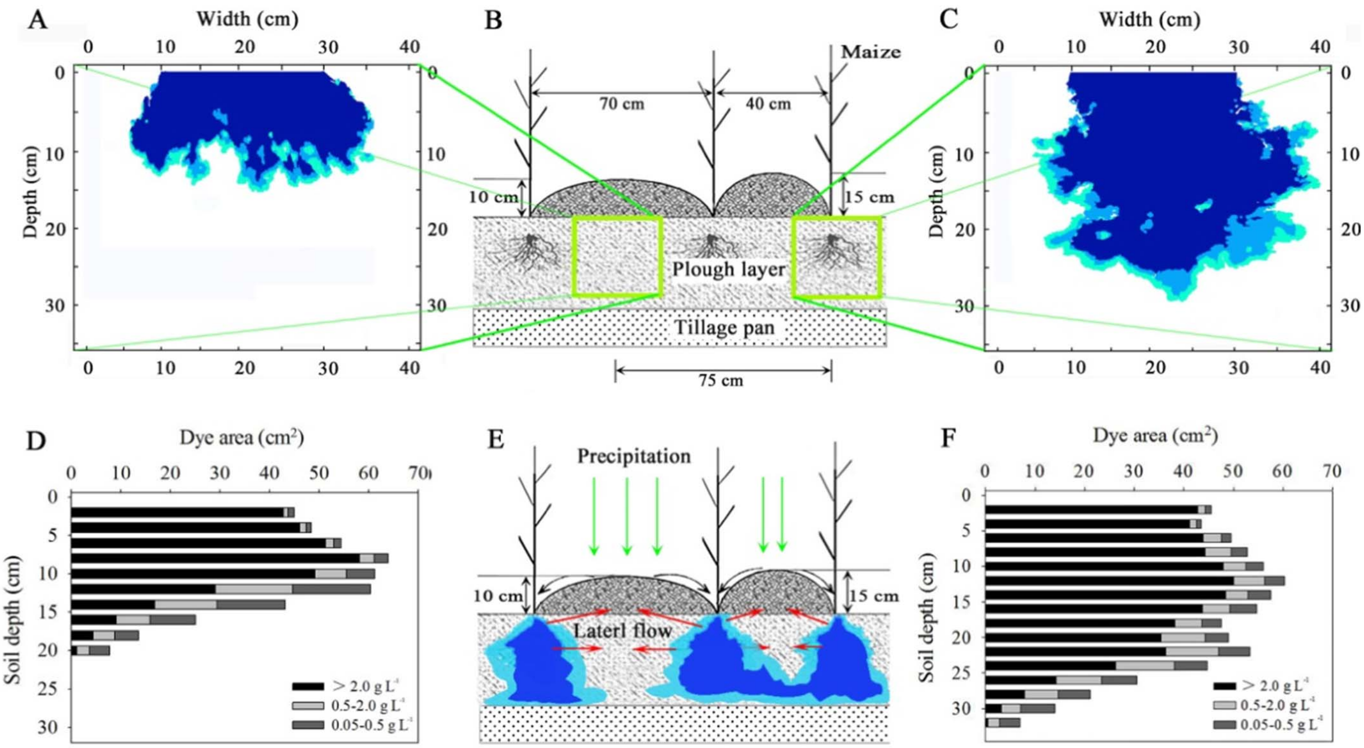

Fig. 4. Infiltration patterns A and C indicated the water flow behaviors in soil without roots and in soil with roots (B), respectively. Real area (cm^2) of the Brilliant Blue FCF dye vs. depth in soil without roots (D) and in soil with roots (F). Potential flow trend of soil water in the pattern of plastic film fully-mulched ridge-furrow cropping during rainfall in Minqin (E). Note: Loose top soil layers of 2 cm and 12 cm were carefully removed from the furrows and ridges, respectively, to prepare quadrants with horizontal surfaces. Thus the findings of the current experiment reflected the water infiltration characteristics in shallow soil not the upper soil layers (which are of vital importance for transmitting water into the soil profile in the first place). (For interpretation of the references to colour in this figure legend, the reader is referred to the web version of this article.)

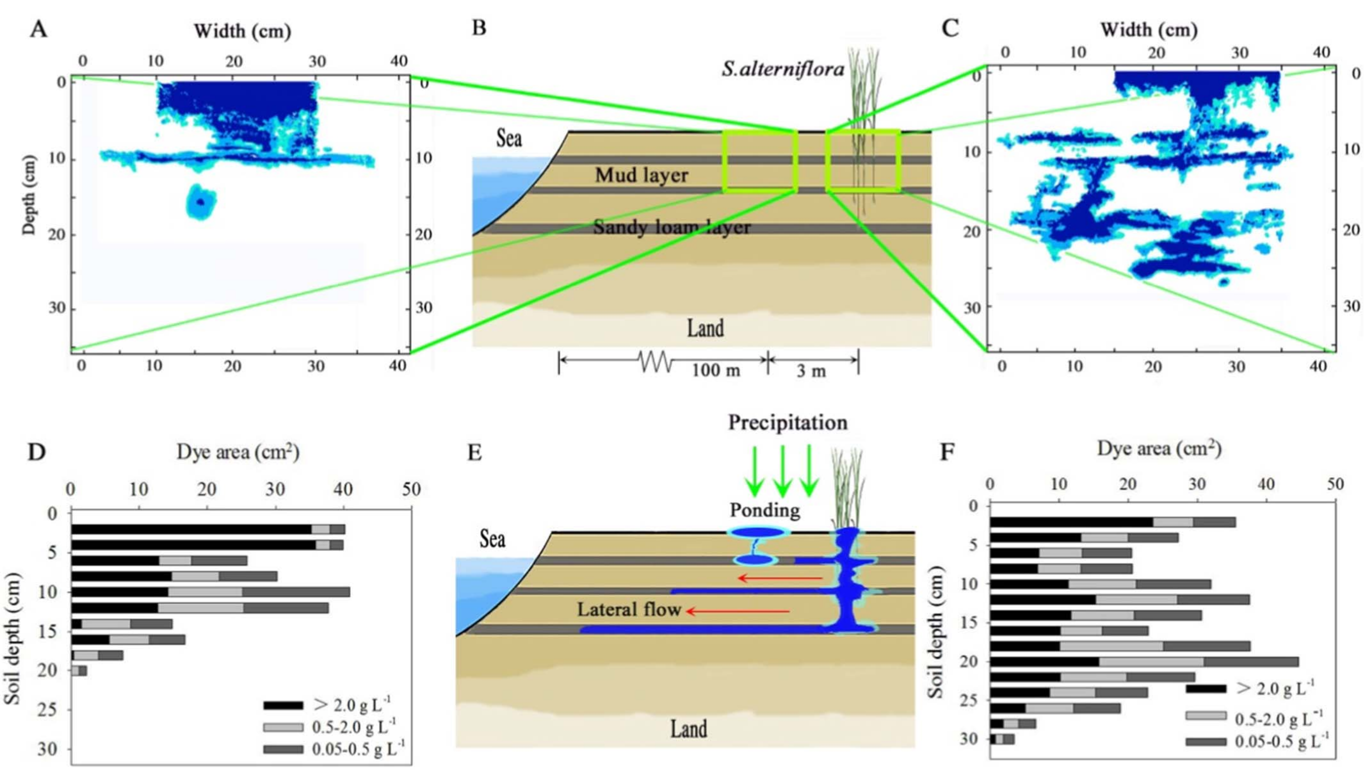

Fig. 5. Infiltration patterns A and C indicated the water flow behaviors in soil without roots and with roots in mud flat (B), respectively. Real area (cm^2) of the Brilliant Blue FCF dye vs. depth in soil without roots (D) and in soil with roots (F). Potential flow trend of soil water during rainfall in Dongtai (E). (For interpretation of the references to colour in this figure legend, the reader is referred to the web version of this article.)

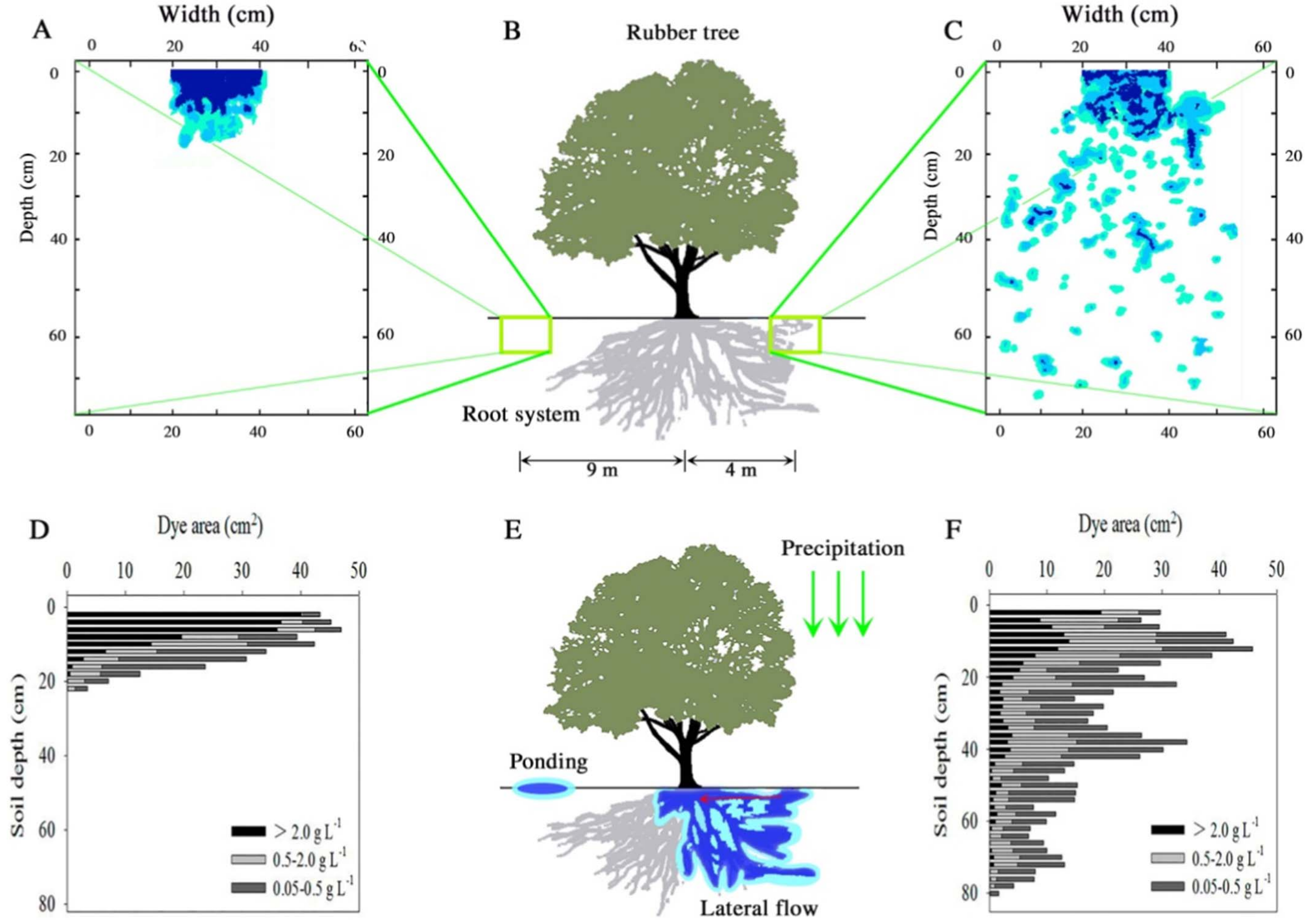

Fig. 6. Infiltration patterns A and C indicated the water flow behaviors in soil without roots and with roots under rubber monoculture crop system (B), respectively. Real area (cm^2) of the Brilliant Blue FCF dye vs. depth in soil without roots (D) and in soil with roots (F). Potential flow trend of soil water during rainfall in Mengla (E). (For interpretation of the references to colour in this figure legend, the reader is referred to the web version of this article.)

sample for each quadrant. The pooled samples were then dried at 105 °C and used for measuring the initial gravimetric water content of the dyed regions.

Image processing was conducted using ERDAS IMAGINE version 9.0 in accordance with the procedures developed by Forrer et al. (2000) and described in detail by Cey and Rudolph (2009). The resulting images were separated into dyed and non-dyed regions. The dyed regions further divided into three relative classes on the basis of dye staining intensity. The dye-stained soil calibration patches were used to determine the concentration categories of the three dye-stained soil classes, that is, 0.05–0.5, 0.5–2.0, and > 2.0 g L^{-1}. The maximum dye-stained depth (cm) and width (cm) of the vertical soil sections were measured using a tapeline. The real area (cm^2) of each concentration category was estimated by counting the stained pixels in the dye staining patterns. Proportion (%) was defined as the percentage of each concentration category over that of the entire stained region in the vertical dye-staining patterns. Addition detailed information on the field measurements and image processing have been provided by Jiang et al. (2015).

2.4. Soil physical properties

Bulk soil samples were acquired and dye infiltration experiments were conducted in three sites that had not experienced rainfall for half a month. Soil physical properties were measured using bulk soil samples (Chen, 2005; Danielson and Sutherland, 1986; Jiao et al., 2011). Bulk soil samples were randomly collected with three replications at depths of 5, 15, 25, and 35 cm with cutting cylinders (inner diameter, 50.46 mm; height, 50.00 mm; volume, 100 cm^3). The mean value of a certain soil property at depths of 5, 15, 25, and 35 cm was used to represent the overall attribute of one plot. The weights of the empty cutting cylinder and the cutting cylinder containing wet soil were recorded as W_{HCR} and W_{CRWS} (g), respectively. In the laboratory, samples were placed in distilled water for saturation. The water was nearly at the level of the soil surface, and no water entered the samples from above. The weight of soil water at saturation (W_{SAT}, g) was measured after the soil core cylinders were ponded for 24 h. Then, the saturated soil core cylinders were placed on sand to measure the weight of water drained through gravity after 2 h and five days (W_{WD2H} and W_{WD5D}, g). Finally, the weight of the cutting cylinder containing dry soil (W_{CRDS}, g) was measured after oven drying at 105 °C for 24 h. Total porosity was calculated in undisturbed water-saturated samples of 100 cm^3 on the assumption that no air was trapped in the pores and validated using dry bulk density and a particle density of 2.65 g cm^{-3} (Danielson and Sutherland, 1986). Then, initial gravimetric water content (%), bulk density (g cm^{-3}), capillary porosity (%) and noncapillary porosity (%) were determined with the following formulae:

$$\textit{Initial gravimetric water content}\ (\%) = \frac{W_{CRWS}\ (\mathrm{g}) - W_{CRDS}\ (\mathrm{g})}{W_{CRDS}\ (\mathrm{g}) - W_{HCR}\ (\mathrm{g})} \times 100$$

$$\textit{Bulk density}\ (\mathrm{g\ cm^{-3}}) = \frac{W_{CRDS}\ (\mathrm{g}) - W_{HCR}\ (\mathrm{g})}{100\ (\mathrm{cm^3})}$$

$$Total\ porosity\ (\%) = \left(1 - \frac{Bulk\ density\ (\mathrm{g\ cm^{-3}})}{Soil\ density\ (\mathrm{g\ cm^{-3}})}\right) \times 100$$

$$Capillary\ holding\ capacity\ (\%) = \frac{W_{WD2H}\,(\mathrm{g}) - W_{CRDS}\,(\mathrm{g})}{W_{CRDS}\,(\mathrm{g}) - W_{HCR}\,(\mathrm{g})} \times 100$$

$$Capillary\ porosity\ (\%) = \frac{Bulk\ density\ (\mathrm{g\ cm^{-3}}) \times Capillary\ holding\ capacity\ (\%)}{\rho_{water}\,(\mathrm{g\ cm^{-3}})}$$

$$Noncapillary\ porosity\ (\%) = Total\ porosity\ (\%) - Capillary\ porosity\ (\%)$$

$$x_s = 100 - Total\ porosity\ (\%)$$

$$x_l = \frac{Initial\ gravimetric\ water\ content\ (\%) \times Bulk\ density\ (\mathrm{g\ cm^{-3}})}{\rho_{water}\,(\mathrm{g\ cm^{-3}})}$$

$$x_g = Total\ porosity\ (\%) - x_I$$

$$TPSI = [(x_s - 25)x_l x_g]^{0.4769}$$

TPSI stands for the three soil phase index, which ranges from 0 to 100 and where x_s is the volumetric solid content (%), x_l is the volumetric water content (%), and x_g is the volumetric gas content (%). TPSI is used to quantify soil physical condition (Wang et al., 2015).

2.5. Statistical analysis

All data were tested for normal distribution. A log-transformation or square root transformation was conducted for nonnormal distribution. One-way ANOVA was applied to assess the effects of roots on dye infiltration parameters and soil physical properties. Spearman's correlation coefficients were used to express the correlation among measured parameters (dye infiltration parameters and soil physical properties). Significant differences between means were detected on the basis of the least significant difference at $P < 0.05$. All statistical procedures were performed in SPSS 20.0. Furthermore, a linear redundancy analysis (RDA) was performed to explore the relationships between dye infiltration parameters and soil physical properties. A Monte Carlo permutation test based on 499 random permutations was conducted to test the significance of the eigenvalues of all canonical axes. All multivariate analyses were conducted using CANOCO 4.5 (ter Braak and Smilauer, 2002).

3. Results

3.1. Fibrous roots of maize

The effects of roots on soil physical properties and dye infiltration patterns are presented in Table 2. In the Minqin site, the soil bulk density of the roots plot decreased by 15% relative to that of the no roots plot. The capillary porosities of the roots plot were 6% higher than those of the no roots plot. Noncapillary porosity increased by 26% in the roots plot compared with that in the no roots plot. Water flow behavior and distribution features were directly interpreted from the vertical dye staining patterns (Fig. 4 A and C). The roots plots exhibited higher numbers of homogeneous dark blue regions with higher concentrations of Brilliant Blue FCF dye than the no roots plots. In addition, the two plots have considerably different dye infiltration parameters. Staining characteristics, such as dye-stained depths, widths, and areas, are summarized in Table 2. Infiltration time decreased by 72% in the roots plot compared with that in the no roots plot. K_s increased by 253% in the roots plot relative to that under the no roots plot. Maximum dye-stained width and depth increased by 26% and 76%, respectively, in the roots plot relative to that in the no roots plot. The total stained area of the roots plot increased by 63% relative to that of the no roots plot. The no roots plot had a small total stained area (422.46 $\mathrm{cm^2}$), of which 65%

Table 2
Effects of roots on measured parameters (mean ± SE, n = 3).

Site	Plot	IGWC (%)	BD ($\mathrm{g\ cm^{-3}}$)	NP (%)	CP (%)	SP (%)	LP (%)	GP (%)	TPSI (%)	IT (min)	K_S ($\mathrm{cm\ s^{-1}}$)	MDSW (cm)	MDSD (cm)	TSA ($\mathrm{cm^2}$)
Minqin	No roots	10.12(0.95)a	1.23(0.01)a	4.18(0.06)b	45.81(0.68)b	50.02(0.65)a	10.12(0.06)b	39.86(0.68)b	81.15(0.47)b	44.51(0.41)a	4.71×10^{-4}b	28.47(1.06)b	16.44(0.60)b	422.46(37.72)b
	Roots	12.47(0.52)a	1.04(0.00)b	5.26(0.04)a	48.56(0.40)a	46.19(0.37)b	12.46(0.31)a	41.35(0.38)a	84.25(0.64)a	12.61(0.40)b	1.66×10^{-3}a	35.74(0.76)a	28.99(0.95)a	686.68(23.73)a
Dongtai	No roots	26.82(0.01)a	1.43(0.02)a	3.81(0.03)b	40.48(0.47)b	38.99(0.33)b	43.07(0.87)a	18.40(1.94)	84.51(2.42)b	1251.0.30(2.51)a	1.67×10^{-5}b	79.95(0.97)a	20.65(0.54)b	256.05(18.49)b
	Roots	26.19(0.37)a	1.25(0.01)b	7.33(1.28)a	54.13(0.24)a	56.01(0.49)a	26.59(0.44)b	17.70(0.28)	96.44(0.46)a	650.65(1.45)b	3.22×10^{-5}a	44.88(1.02)b	28.29(0.32)a	389.73(57.09)a
Mengla	No roots	24.42(0.68)a	1.43(0.02)a	1.13(0.03)b	40.43(0.47)b	58.45(0.49)a	26.59(0.44)b	14.96(0.28)b	92.60(0.46)b	1445.00(32.93)a	8.67×10^{-7}b	22.05(0.97)b	18.58(0.54)b	328.36(18.49)b
	Roots	26.78(0.53)a	1.34(0.01)b	3.77(0.06)a	44.04(0.77)a	52.20(0.82)b	30.37(0.88)a	17.44(0.96)a	95.99(0.97)a	735.20(35.55)b	1.70×10^{-6}a	52.51(2.29)a	73.54(1.94)a	786.27(44.74)a

IGWC, initial gravimetric water content. BD, bulk density. NP, noncapillary porosity. CP, capillary porosity. SP, solid phase. LP, liquid phase. GP, gas phase. TPSI, three soil phase index. IT, infiltration time. MDSW, maximum dye-stained width. MDSD, maximum dye-stained depth. TSA, total stained area.
Different letters within one column indicate a significant difference at $p < 0.05$.

was confined to the upper 10 cm of the soil profile. The roots plot had a large total stained area (686.68 cm^2), of which 75% was confined to the upper 20 cm of the soil profile. The quantitative information of infiltration behavior illustrated that stained area (cm^2) varied with soil depth (Fig. 4 D and F). Stained area consistently increased from the soil surface (0 cm) to the depth of 10 cm. Stained area in the no roots plot increased by a larger extent than those in the roots plot. After the depth of 10 cm, stained areas in the no roots plot sharply decreased, whereas those in the roots plot gradually decreased.

3.2. Smooth roots of *S. alterniflora*

In the Dongtai site, the soil bulk density of the roots plot decreased by 13% relative to that of the no roots plot. The capillary porosities of the roots plot were 34% higher than those of the no roots plot. Noncapillary porosity in the roots plot decreased by 63% of that in the no roots plot. The vertical dye staining patterns of the no roots plot exhibited numerous homogeneous dark blue regions (Fig. 5 A and C). Infiltration parameters differed between the roots and no roots plots. Infiltration time in the roots plot decreased by 48% relative to that in the no roots plot (Table 2). K_s increased by 92% in the roots plot relative to that in the no roots plot. Maximum dye-stained width decreased by 44% in the roots plot relative to that in the no roots plot. Maximum dye-stained depth in the roots plot increased by 37% relative to that in the no roots plot. The total stained area in the roots plot increased by 52% relative to that in the no roots plot. The no roots plot had a low total stained area (256.05 cm^2), 69% of which was confined to the upper 10 cm of the soil profile. The roots plot had a high total area (389.73 cm^2), 79% of which was confined to the upper 20 cm of the soil profile. Stained area (cm^2) varied with soil depth. These variations match those exhibited by the vertical dye staining patterns (Fig. 5 D and F). The alternating decrease and increase in stained areas with soil depth was less apparent in the no roots plot than in the roots plot.

3.3. Fine roots of rubber

In the Mengla site, soil bulk density in the roots plot decreased by 7% relative to that in the no roots plot. Capillary porosities in the roots plot were 9% higher than those in the no roots plot. Noncapillary porosity increased by 234% in the roots plot compared with that in the no roots plot. Water flow behavior and distribution features were directly interpreted from the vertical dye staining patterns (Fig. 6 A and C). Dye-stained patterns in the no roots plot were confined to the upper 20 cm of the soil profile, whereas those in the roots plot were randomly scattered. Infiltration time and K_s in the roots plot decreased by 49% and increased by 96%, respectively, relative to those in the no roots plot (Table 2). Maximum dye-stained width and depth in the roots plot increased by 138% and 296%, respectively, relative to that in the no roots plot. The total stained area in the roots plot increased by 139% relative to that in the no roots plot. The no roots plot exhibited a low total stained area (328.36 cm^2), of which 67% was confined to the upper 10 cm of the soil profile. The roots plot had a high total stained area (786.27 cm^2), of which 43% was confined to the upper 20 cm of the soil profile. In the no roots plot, the stained area consistently decreased from the soil surface (0 cm). By contrast, the stained area in the roots plot alternately decreased and increased with increasing depth (Fig. 6 D and F).

In the Minqin site, the final gravimetric water content (measured after infiltration was completed) of the no roots and roots plots increased by 61% and 51%, respectively, relative to their initial gravimetric water content. In the Dongtai site, the final gravimetric water content of the stained regions in the mud layer increased by 54% in the no roots plot and by 52% in the roots plot relative to their initial gravimetric water content. Meanwhile, the final gravimetric water content of the stained regions in the sandy loam layer increased by 12% in the no roots plot and 19% in the roots plot relative to their initial gravimetric water content. More importantly, mud and sandy loam layers had similar values for initial gravimetric water content; however, the final gravimetric water content of the stained regions in the mud layer was 50% higher than those of stained regions in the sandy loam layer. In the Mengla site, the final gravimetric water content of the no roots and roots plots increased by 37% and 21%, respectively, relative to their initial gravimetric water content.

4. Discussion

4.1. Effect of roots on soil water flow behavior

The measured parameters of the plots in the Minqin site implied that furrows (roots plot) and ridges (no roots plot) exhibit different soil physical properties and water infiltration characteristics. Consistent with the findings by Armand et al. (2009) and Jabro et al. (2009), the furrows and ridges in the cultivated field exhibited different soil bulk density, capillary porosity, and noncapillary porosity. Preferential flow has been observed in fields under conservation and conventional (Jiang et al., 2015) tillage and under uncultivated conditions (Jiang et al., 2017a). However, the dominant type of water flow through furrows and ridges is unclear. In this study, we found that preferential flow is the dominant type of water flow in furrows and ridges. Fibrous maize roots provided the dominant path for preferential flow in furrows, whereas macropores provided the dominant path for preferential flow in the loose and fragmented soil structure of ridges. The dye tracer experiment highlighted that water infiltration occurred from the inner soil layers of furrows to the inner soil layers of ridges (Fig. 4 E). Quantitative and qualitative data provided direct evidence for the previous assumption that in the field, soil water is transported from wet soil in furrows to dry soil in ridges (Wu et al., 2016). More importantly, lateral flow from furrows to ridges could be enhanced by tillage pan, which is subjected to compaction (Jiang et al., 2015). This finding indicated that rainwater could be collected, distributed, and stored in the deep soil layers of furrows. Plastic mulching could weaken evaporation and enhance water exchange between furrows and ridges. Therefore, the cropping pattern of film-mulched furrow–ridge could effectively increase water use from rainfall by crops in semiarid areas.

In the Dongtai site, the no roots plot had a bulk density of 1.43 $g\,cm^{-3}$ and extremely high initial gravimetric water content (25.51% in sandy soil and 27.82% in mud soil). The water content of stained regions in the mud layer was higher than that of stained regions in the sandy loam layer and approached the value of saturated water-holding capacity. This result implied that the mud layer is characterized by low hydraulic conductivity, whereas the sandy loam layer is characterized by high hydraulic conductivity. A considerable proportion of the stained areas in the no roots plot were confined to the upper 10 cm soil layer. This result corresponded with the findings of Hamed (2008), who noted that dye easily penetrates the upper mud layer and that 70% of the stained areas are confined to the upper 10 cm layer of soil. However, only 20% of the stained areas are found at depths of 10 cm to 20 cm. Hamed (2008) attributed the decrease in dye coverage to two reasons: First, numerous macropores and cracks accumulate at the surface of the mud layer. Second, water slowly permeates through the mud layer. For example, in the present study, the dye tracer required three days to permeate through the mud layer. Dye-stained areas were evenly distributed throughout the profiles of the roots plots (Fig. 5 A). The hydrologic process in soil is closely connected with soil structure. In the Dongtai site, water infiltration was inhibited by the mud layer, consequently resulting in ponding and surface runoff. These phenomena, however, were not observed in sites wherein the pond layer was penetrated by numerous roots, which could provide potential paths for preferential flow between the mud and sandy loam layers. Lateral flow in sandy loam layers surrounded by two mud layers encountered high hydraulic pressure. These results provided evidence for the

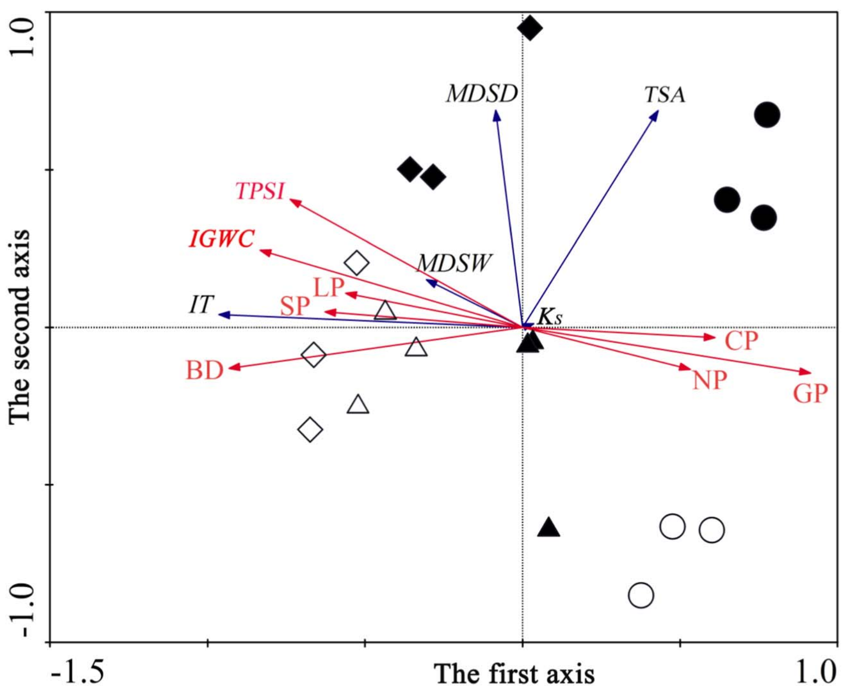

Fig. 7. Ordination diagram showing the results of RDA of soil physical properties and dye infiltration parameters. Hollow and solid points represent no roots and roots plots, respectively. Triangle, circle, and rhombus represent Dongtai, Minqin, Mengla respectively. IGWC, initial gravimetric water content. BD, bulk density. NP, non-capillary porosity. CP, capillary porosity. SP, solid phase. LP, liquid phase. GP, gas phase. TPSI, three soil phase index. IT, Infiltration time. *Ks*, saturated hydraulic conductivity. MDSW, maximum dye-stained width. MDSD, maximum dye-stained depth. TSA, total stained area.

viewpoints of Sarmah and Barua (2015), who considered that alternating mud and sandy loam layers can lead to the development of a uniform flow field and increase water infiltration in a drainage system. In addition, macropores created by plant roots in the upper soil layer act as drains as the tide ebbs and as recharge wells as the tide rises (Fig. 5 E). Therefore, the present results implied that water infiltration behavior, that is, preferential flow induced by smooth fine roots and lateral flow triggered by the sandy loam layer, is of considerable importance to water recharge in the Dongtai site.

The capillary and noncapillary porosities of the roots plot in the Mengla site were higher than that in the no roots plot. This result is in agreement with that previously reported by Maggiotto et al. (2014). Roots improve soil physical properties through several distinct ways. Decaying and dead roots components could provide spaces for water and air storage in soil. In addition, Barzegar et al. (2002) noted that certain patterns of roots distribution and penetration could improve soil physical properties, such as bulk density. For example, short-lived and non-woody fine plant roots can generate additional paths for preferential flow. During roots penetration, soil particles may reorganize around the roots surface to form a coating of clay particles on the sides of the roots channel. More importantly, the physical, chemical, and biological characteristics of the rhizosphere, which is defined as the assemblage of roots, microorganisms, and soil around roots with the exception of bulk soil (Tarafdar and Jungk, 1987), differ from those of rootless soil. Numerous researchers have stated that an important characteristic of preferential flow is that during wetting, sections of the moisture front can rapidly propagate to significant depths while bypassing a considerable portion of the matrix pore space (Benegas et al., 2014; Flury and Flühler, 1994; Hendrickx and Flury, 2001; Kung, 1990). This important characteristic was also observed in the Mengla site. Moreover, preferential flow in this site was not driven by gravity. This special phenomenon could be attributed to two reasons: First, water could flow in the heterogeneous interface between the rhizopore (the cylindrical space around the roots) and its surrounding soil. Second, the fine roots of rubber trees could guide and promote water infiltration into deep soil layers. In addition, soil became compacted (bulk density in the roots and no roots plot reached up to 1.34 and 1.43 g cm^{-3}, respectively) because of the frequent trampling of the soil surface (Yi et al., 2014). Thus, water infiltration in this site required a long time (12.25 and 24.08 h for the roots and no roots plots, respectively). The randomly scattered stained areas and the long duration and deep penetration of infiltration indicated that this water infiltration behavior is inconsistent with conventional preferential flow. Gardner (1979) believed that gravity and adhesion (cohesion) are the two major forces that move water through soil pores. Obviously, gravity was not the main driving force of water movement in the Mengla site. Adhesion (cohesion), which causes water molecules to stay together, could drive water to move along particle surfaces and through fine pores. This force is similar to capillary force, which causes water to rise and migrate in capillary tubes (Wu et al., 2017). The fine roots of rubber trees likely act as capillary tubes. Therefore, adhesion and capillary tubes likely promote the movement of soil water through the soil profile of the Mengla site. Water infiltration in the no roots plot was confined to the upper 10 cm of the soil profile, and matrix flow was the dominant flow type. Water flow induced by fine roots could be slowly transported along the distribution of fine roots. Specifically, the distribution regions of soil water corresponded to the distribution regions of fine roots. Therefore, water was supplied to rubber trees through slow flow, which could be enhanced by the dynamic activities of fine roots and the rhizosphere (Fig. 6 E).

4.2. Correlation between soil physical properties and water infiltration features

Mitchell (1995) and Benegas et al. (2014) reported that tree roots (living and decaying) positively affect soil infiltration by increasing macroporosity and soil aggregation. Our results confirmed that roots significantly reduce soil bulk density and increase total porosity and saturated hydraulic conductivity. However, few researchers have studied the relationships between roots and dye infiltration parameters. Our work showed differences between roots and no roots plots. For example, in the Minqin site, the maximum dye-stained width, maximum dye-stained depth, and total stained area of the roots plot are higher than those of the no roots plot. In general, the averaged values of the three sites indicated that the presence of roots significantly affect bulk density, noncapillary porosity, infiltration time, K_s, maximum dye-stained width, maximum dye-stained depth, and total stained area.

We also found that the correlation among soil physical properties

Table 3
Correlation coefficients of soil physical properties and dye infiltration parameters. The value was a general mean for the three sites.

Indicator	Initial gravimetric water content	Bulk density	Noncapillary porosity	Capillary porosity	Solid phase	Liquid phase	Gas phase	Three soil phase index
Infiltration time	0.603**	0.926**	−0.740**	−0.779**	0.796**	0.414	−0.926**	0.647**
K_s	−0.532*	−0.877**	0.756**	0.684**	−0.713**	−0.498*	0.902**	−0.665**
MDSW	0.758**	0.179	0.148	−0.036	−0.065	0.430	−0.009	0.474*
MDSD	0.430	−0.156	0.264	0.325	−0.356	0.623**	0.014	0.349
TSA	−0.198	−0.540*	0.226	0.459	−0.404	0.009	0.447	−0.073

MDSW, maximum dye-stained width. MDSD, maximum dye-stained depth. TSA, total stained area.
* $P < 0.05$.
** $P < 0.01$.

and dye infiltration parameters was specific to different sites. For example, the positive relationship between infiltration time and initial gravimetric water content was specific to the Mengla site (Fig. 7, Table 3). Total stained area was most correlated with two RDA axes. The maximum dye-stained width was positively related with the second RDA axis. Infiltration time was negatively related with the first RDA axis. Kuncoro et al. (2014) found that total porosity and saturated hydraulic conductivity are positively and linearly related, which is in accordance with our results. More importantly, we found that soil physical properties and dye infiltration parameters were significantly correlated (Table 3). K_s was strongly positively related with noncapillary porosity ($r = 0.756$, $p < 0.001$) and capillary porosity ($r = 0.684$, $p = 0.002$) and was strongly negatively related with initial gravimetric water content ($r = 0.532$, $p = 0.023$), bulk density ($r = 0.877$, $p < 0.001$), and three-soil phase index ($r = 0.665$, $p = 0.003$). The maximum dye-stained width was strongly and positively related with initial gravimetric water content ($r = 0.758$, $p < 0.001$) and three-soil phase index ($r = 0.474$, $p = 0.047$). These associations could be attributed to the influence of roots on soil physical properties, which influence dye infiltration parameters.

5. Conclusions

The results of our study highlighted that water infiltration behavior, which is affected by the variations in the morphometric features of different roots, is crucial to water distribution. In the Minqin site, fibrous maize roots provided the dominant path for preferential flow in furrows, whereas macropores provided the dominant path for preferential flow in the loose and fragmented soil structure of ridges. Lateral flow from the inner soil layers of furrows to those of ridges, as well as variations in soil porosities, resulted in the even distribution of water in furrows and ridges. In the Dongtai site, water infiltration was inhibited by the mud layer, subsequently resulting in ponding and surface runoff. These phenomena, however, were not observed in sites where the smooth roots of *S. alterniflora* penetrated the mud layer and could potentially provide paths for preferential flow between two soil layers. Preferential and lateral flows, which occur in the sandy loam layers between two mud layers, are crucial for discharging water from the beach to the ocean. In the Mengla site, portions of the moisture front propagated to significant depths while bypassing large areas of the matrix pore space. Randomly scattered dye-stained areas in the soil profile and the long duration and deep penetration of water infiltration indicated that the fine roots of rubber trees could guide and promote water infiltration into the deep soil layers of this site.

Acknowledgments

We thank the Central Laboratory of XTBG for their help. This research was supported by the project of National Natural Science Foundation of China (41701029 and 31570622), the project of Natural Science Foundation of Yunnan Province (2014HB042), the CAS 135-Program (No. 2017XTBG-F01), and the Youth Innovation Promotion Association CAS.

References

Allaire, S.E., Roulier, S., Cessna, A.J., 2009. Quantifying preferential flow in soils: a review of different techniques. J. Hydrol. 378, 179–204.
Armand, R., Bockstaller, C., Auzet, A.V., Van Dijk, P., 2009. Runoff generation related to intra-field soil surface characteristics variability: application to conservation tillage context. Soil Tillage Res. 102, 27–37.
Barzegar, A.R., Yousefi, A., Daryashenas, A., 2002. The effect of addition of different amounts and types of organic materials on soil physical properties and yield of wheat. Plant Soil 247, 295–301.
Benegas, L., Ilstedt, U., Roupsard, O., Jones, J., Malmer, A., 2014. Effects of trees on infiltrability and preferential flow in two contrasting agroecosystems in central America. Agric. Ecosyst. Environ. 183, 185–196.
Beven, K., Germann, P., 1982. Macropores and water flow in soils. Water Resour. Res. 18, 1311–1325.
Bodhinayake, W., Si, B.C., Noborio, K., 2004. Determination of hydraulic properties in sloping landscapes from tension and double-ring infiltrometers. Vadose Zone J. 3, 964–970.
Bond, R.D., 1964. The influence of the microflora on the physical properties of soils. II. Field studies on water repellent sands. Soil Res. 2, 123–131.
Bond, R.D., Harris, J.R., 1964. The influence of the microflora on the physical properties of soils. I. Effects associated with filamentous algae and fungi. Soil Res. 2, 111–122.
ter Braak, C.J.F., Smilauer, P., 2002. CANOCO Reference Manual and User's Guide to Canoco for Windows: Software for Canonical Community Ordination (Version 4.5). Micro-Computer Power, Ithaca, NY, US.
Bundt, M., Widmer, F., Pesaro, M., Zeyer, J., Blaser, P., 2001. Preferential flow paths: biological 'hot spots' in soils. Soil Biol. Biochem. 33, 729–738.
Castellano, M.J., Valone, T.J., 2007. Livestock, soil compaction and water infiltration rate: evaluating a potential desertification recovery mechanism. J. Arid Environ. 71, 97–108.
Cey, E.E., Rudolph, D.L., 2009. Field study of macropore flow processes using tension infiltration of a dye tracer in partially saturated soils. Hydrol. Process. 23, 1768.
Chen, L.X., 2005. Soil Test Course. Northeast forestry university press, Harbin (In Chinese.).
Czarnes, S., Hallett, P.D., Bengough, A.G., Young, I.M., 2000. Root-and microbial-derived mucilages affect soil structure and water transport. Eur. J. Soil Sci. 51, 435–443.
Danielson, R.E., Sutherland, P.L., 1986. Porosity. In: Methods of Soil Analysis: Part 1—Physical and Mineralogical Methods, pp. 443–461 (methodsofsoilan1).
DeBano, L.F., Dunn, P.H., Conrad, C.E., 1977. Fire's Effect on Physical and Chemical Properties of Chaparral Soils. (USDA Forest Service General Technical Report WO).
Fleischner, T.L., 1994. Ecological costs of livestock grazing in western North America. Conserv. Biol. 8, 629–644.
Flury, M., Flühler, H., 1994. Brilliant blue FCF as a dye tracer for solute transport studies-a toxicological overview. J. Environ. Qual. 23, 1108–1112.
Flury, M., Flühler, H., 1995. Tracer characteristics of brilliant blue FCF. Soil Sci. Soc. Am. J. 59, 22–27.
Forrer, I., Papritz, A., Kasteel, R., Flühler, H., Luca, D., 2000. Quantifying dye tracers in soil profiles by image processing. Eur. J. Soil Sci. 51, 313–322.
Gardner, W.H., 1979. How water moves in the soil. Crop. Soil 32, 13–18.
Ghestem, M., Sidle, R.C., Stokes, A., 2011. The influence of plant root systems on subsurface flow: implications for slope stability. Bioscience 61, 869–879.
Ghodrati, M., Jury, W.A., 1990. A field study using dyes to characterize preferential flow of water. Soil Sci. Soc. Am. J. 54, 1558–1563.
Gibbs, R.J., Reid, J.B., 1988. A conceptual model of changes in soil structure under different cropping systems. In: Advances in Soil Science. Springer, New York, pp. 123–149.
Hamed, K.H., 2008. Trend detection in hydrologic data: the Mann-Kendall trend test under the scaling hypothesis. J. Hydrol. 349, 350–363.
Hendrickx, J.M., Flury, M., 2001. Uniform and preferential flow mechanisms in the vadose zone. In: Conceptual Models of Flow & Transport in the Fractured Vadose Zone, pp. 149–187.
IUSS Working Group WRB, 2014. World Reference Base for Soil Resources 2014: International Soil Classification System for Naming Soils and Creating Legends for Soil Maps. World Soil Resources Reports 106. FAO, Rome.
Jabro, J.D., Stevens, W.B., Evans, R.G., Iversen, W.M., 2009. Tillage effects on physical properties in two soils of the Northern Great Plains. Appl. Eng. Agric. 25, 377.
Jiang, X., Liu, X., Wang, E., Li, X.G., Sun, R., Shi, W., 2015. Effects of tillage pan on soil water distribution in alfalfa-corn crop rotation systems using a dye tracer and geostatistical methods. Soil Tillage Res. 150, 68–77.

Jiang, X.J., Liu, S., Zhang, H., 2017a. Effects of different management practices on vertical soil water flow patterns in the Loess Plateau. Soil Tillage Res. 166, 33–42.
Jiang, X.J., Liu, W., Wang, E., Zhou, T., Xin, P., 2017b. Residual plastic mulch fragments effects on soil physical properties and water flow behavior in the Minqin Oasis, northwestern China. Soil Tillage Res. 166, 100–107.
Jiang, X.J., Liu, W., Wu, J., Wang, P., Liu, C., Yuan, Z.Q., 2017c. Land degradation controlled and mitigated by rubber–based agroforestry systems through optimizing soil physical conditions and water supply mechanisms: a case study in Xishuangbanna, China. Land Degrad. Dev. 28, 2277–2289.
Jiao, F., Wen, Z.M., An, S.S., 2011. Changes in soil properties across a chronosequence of vegetation restoration on the Loess Plateau of China. Catena 86, 110–116.
Kodešová, R., Němeček, K., Kodeš, V., Žigová, A., 2012. Using dye tracer for visualization of preferential flow at macro-and microscales. Vadose Zone J. 11, 12–22.
Kuncoro, P.H., Koga, K., Satta, N., Muto, Y., 2014. A study on the effect of compaction on transport properties of soil gas and water I: relative gas diffusivity, air permeability, and saturated hydraulic conductivity. Soil Tillage Res. 143, 172–179.
Kung, K.S., 1990. Preferential flow in a sandy vadose zone: 2. Mechanism and implications. Geoderma 46, 59–71.
Laine-Kaulio, H., Backnäs, S., Koivusalo, H., Lauren, A., 2015. Dye tracer visualization of flow patterns and pathways in glacial sandy till at a boreal forest hillslope. Geoderma 259, 23–34.
Lipiec, J., Kuś, J., Słowińska-Jurkiewicz, A., Nosalewicz, A., 2006. Soil porosity and water infiltration as influenced by tillage methods. Soil Tillage Res. 89, 210–220.
Maggiotto, S.R., Oliveira, D.D., Marur, C.J., Stivari, S.M.S., Leclerc, M., Wagner-Riddle, C., 2014. Potential carbon sequestration in rubber tree plantations in the northwestern region of the Paraná state. Brazil. Acta Sci-Agron. 36, 239–245.
Mallik, A.U., Gimingham, C.H., Rahman, A.A., 1984. Ecological effects of heather burning: I. Water infiltration, moisture retention and porosity of surface soil. J. Ecol. 767–776.
McGarry, D., Bridge, B.J., Radford, B.J., 2000. Contrasting soil physical properties after zero and traditional tillage of an alluvial soil in the semi-arid subtropics. Soil Tillage Res. 53, 105–115.
Mitchell, W.T., 1995. Picture Theory: Essays on Verbal & Visual Representation. University of Chicago Press.
Oostindie, K., Dekker, L.W., Wesseling, J.G., Ritsema, C.J., Geissen, V., 2013. Development of actual water repellency in a grass-covered dune sand during a dehydration experiment. Geoderma 204, 23–30.
Reynolds, W.D., Elrick, D.E., 1990. Ponded infiltration from a single ring: I. Analysis of steady flow. Soil Sci. Soc. Am. J. 54 (5), 1233–1241.
Reynolds, W.D., Lewis, K.L., 2012. A drive point application of the Guelph Permeameter method for coarse-textured soils. Geoderma 187, 59–66.
Ritsema, C.J., Dekker, L.W., 1995. Distribution flow: a general process in the top layer of water repellent soils. Water Resour. Res. 31, 1187–1200.
Sarmah, R., Barua, G., 2015. Hydraulics of a partially penetrating ditch drainage system in a layered soil receiving water from a ponded field. J. Irrig. Drain. Eng. 141, 04015001.
Tarafdar, J.C., Jungk, A., 1987. Phosphatase activity in the rhizosphere and its relation to the depletion of soil organic phosphorus. Biol. Fertil. Soils 3, 199–204.
Tebrügge, F., Düring, R.A., 1999. Reducing tillage intensity-a review of results from a long-term study in Germany. Soil Tillage Res. 53, 15–28.
Vogel, A.W., Wang, M.Z., Huang, X.Q., 1995. People's Republic of China: red reference soil of tropical southern Yunnan province. In: Soil Brief China 1. Institute of Soil Science-AcademicaSinica, Nanjing, and International Soil Reference and Information Center, Wageningen.
Wang, R.Y., Strong, D.M., 1996. Beyond accuracy: what data quality means to data consumers. J. Manag. Inf. Syst. 12, 5–33.
Wang, E., Cruse, R.M., Zhao, Y., Chen, X., 2015. Quantifying soil physical condition based on soil solid, liquid and gaseous phases. Soil Tillage Res. 146, 4–9.
Weiler, M., Flühler, H., 2004. Inferring flow types from dye patterns in macroporous soils. Geoderma 120, 137–153.
Wine, M.L., Ochsner, T.E., Sutradhar, A., Pepin, R., 2012. Effects of eastern redcedar encroachment on soil hydraulic properties along Oklahoma's grassland-forest ecotone. Hydrol. Process. 26, 1720–1728.
Wu, Y., Du, T., Li, F., Li, S., Ding, R., Tong, L., 2016. Quantification of maize water uptake from different layers and root zones under alternate furrow irrigation using stable oxygen isotope. Agr. Water Manage. 168, 35–44.
Wu, J., Liu, W., Chen, C., 2017. How do plants share water sources in a rubber-tea agroforestry system during the pronounced dry season? Agric. Ecosyst. Environ. 236, 69–77.
Xin, P., Yu, X., Lu, C., Li, L., 2016. Effects of macro-pores on water flow in coastal subsurface drainage systems. Adv. Water Resour. 87, 56–67.
Yi, Z.F., Cannon, C.H., Chen, J., Ye, C.X., Swetnam, R.D., 2014. Developing indicators of economic value and biodiversity loss for rubber plantations in Xishuangbanna, southwest China: a case study from Menglun township. Ecol. Indic. 36, 788–797.